Large Scale Lattice-Boltzmann Simulations: Computational Methods and Applications

Kandhai, B.D.

Publication date
1999

Addendum A

Finite-Difference Lattice-BGK Methods on Nested Grids

A.1 Introduction

In recent years the Lattice-Boltzmann method [12, 28, 80] has attracted much attention in the simulation of complex fluid flow problems. Typical examples are fluid flow in porous media, multi-phase flow and particle suspension flow (see e.g. Refs. [12, 16, 40]). The success of this method can be partly attributed to the particle based approach which is directly inherited from its predecessor, the lattice-Gas model [13].

Although the scheme has proven to be very promising, it has some potential shortcomings compared to traditional state of the art numerical methods, like the Finite-Element method. The uniformity of the lattice is argued to be one of them (see e.g. Ref. [29]). From a computational point of view non-uniform grids can be efficient for computing fluid flows because the grid resolution can be adapted to the spatial complexity of the flow dynamics.

The lattice-Boltzmann method evolved from the early lattice-Gas model where particles hop from one lattice site to one of its neighbors, constrained to mass and momentum conservation. In these models a discrete set of velocities is used that is directly connected with the topology of the computational lattice. Correct macroscopic behavior is only guaranteed when the symmetry properties of the computational lattice are such that the transport coefficients are isotropic. The lattice-Boltzmann model automatically inherited this constraint imposed on the lattice from its predecessor.

In this addendum we introduce an alternative approach, allowing LBM simulations on non-uniform grids. In our approach, the computational grid consists of multiple nested grids with increasing spatial resolution. Basically, the discrete velocity Boltzmann equation (see next section) is solved numerically on each sub-lattice and interpolation between the interfaces is carried out in order to couple the sub-grids consistently. The approach is validated for the Taylor vortex flow problem.

A.2 Background

In this section we present a brief overview of the main developments related to non-uniform grids for the Lattice-Boltzmann method. One of the first attempts to generalize the lattice-Boltzmann scheme to non-uniform grids has been reported by Nanneli and Succi [69]. In their approach a finite volume strategy is studied. The non-uniform grid consists of cells corresponding to several grid points in the original lattice. For each cell, a volume-average particle distribution is defined. By using piece-wise constant or linear interpolation methods the coarse grain distribution is approximated. Using this approach reasonable results were found for laminar flow in a channel.

More recently, a different approach for handling non-uniform grids has been proposed by He and Luo [86]. In their method the grids on which the propagation step is performed is decoupled from that of the collision phase. After each propagation step the particle densities are interpolated to the original mesh or grid and then the collision phase in carried out. It was shown, that the quality of this approach is highly determined by the interpolation scheme used [86].

A few years ago, Cao et al. [29] argued that although the physical symmetry (related to the collision phase) and the lattice symmetry (related to the propagation phase) are equivalent for LGA they may be different for Lattice-Boltzmann Models (LBM). LBM can be viewed as a special finite-difference discretization of the single time relaxation approximation of the Boltzmann equation for discrete velocities,

$$\frac{\partial f_i}{\partial t} + \mathbf{e}_i \cdot \nabla f_i = \Omega_i \qquad (i = 1, 2, ..., N), \tag{A.1}$$

where f_i is the particle velocity distribution, $\mathbf{e}_i$ is the velocity along the i-th direction, N is the number of different velocities, and Ω_i represents the collision operator. By applying a first-order Euler time differencing scheme, a first-order upwind space discretization for the convection term in Eq. A.1, splitting the collision and convection process into two separate steps, and setting the lattice spacing Δx equal to the time step Δt, the standard Lattice-BGK (LBGK) model can be derived [29]. Although both the time and space discretization schemes are first-order the LBGK model is second-order both in time and space, because the numerical viscosity has a special form which can be included in the fluid viscosity.

The important consequence is that in the LBGK model one can now incorporate arbitrary grids in the scheme by exploiting a different time and space discretization then the ones used above (the so-called Finite Difference Lattice-Boltzmann method). Based on this idea Cao et al. [29] proposed the LBGK method on cylindrical coordinates using central difference methods for the space discretization. Later, Mei and Shyy extended these studies to more complicated body fitted coordinates [120]. And recently, Peng et al. formulated a finite volume scheme for the lattice-Boltzmann method on unstructured meshes based on the Boltzmann equation for discrete velocities [121].

In this addendum we discuss a generalization of the method proposed by Cao

et al. [29] to nested grids. The computational grid is basically built up of a number of sub-domains which can have different grid resolutions. On each sub-domain the discrete velocity Boltzmann equation is solved and the adjacent sub-domains are coupled which each other by appropriate interpolation at the boundaries of the sub-domains. We think that such a generalization might be very useful, because the method is still closely related to the spirit of standard LBGK algorithm and thus it is expected that more complex LBM models (multiphase- or thermal models) can still be used in this framework.
We also point out that the formulation of LBM on nested grids has been studied by Fillipova and Hanel [122]. Their approach is based on the LBGK method, whereas we start from the Boltzmann equation for discrete velocities. We will discuss their method in some more detail in section IV.
We first discuss, in section II, the discretization of Eq. A.1. Next, in section III, we introduce the extension of the Lattice Boltzmann scheme on nested grids. We discuss the data structures and a consistent coupling between the different grids. Finally, in section IV, we present some preliminary numerical results.

A.3 Numerical Discretization of the Boltzmann Equation

As argued in the previous section, in our approach the Boltzmann equation for a discrete set of velocities (Eq. A.1) is solved numerically. The numerical discretization consists of a spatial discretization of the convection operator and a time integration of Eq. A.1. The collision operator is defined locally on each lattice point analogous to the standard LBM method. For the spatial discretization we use second-order central-difference and upwind schemes and for the temporal discretization a second-order Runge Kutta method is used.
In this section we review the finite difference schemes. For simplicity we only consider the equation for the velocity pointing to the right neighbor, denoted by index 1. The second-order upwind scheme for link 1 is given by,

$$\frac{\partial f_1}{\partial x} = \frac{(3f_1(x,y) - 4f_1(x-\Delta x,y) + f_1(x-2\Delta x,y))}{2\Delta x}, \tag{A.2}$$

where Δx is the lattice spacing in the x-direction. The central difference scheme is given by,

$$\frac{\partial f_1}{\partial x} = \frac{(f_1(x+\Delta x,y) - f_1(x-\Delta x,y))}{2\Delta x}. \tag{A.3}$$

The molecular velocities, $\mathbf{e}_i$ are in fact free but restricted by stability constraints. In the standard LBGK method they are defined as $\mathbf{e}_i = (cos(\frac{\pi}{2}(i-1)), sin(\frac{\pi}{2}(i-1)))\frac{\Delta x}{\Delta t}$ for $i = 1,2,3,4$ and $\mathbf{e}_i = \sqrt{2}(cos(\frac{\pi}{2}(i-5)+\frac{\pi}{4}), sin(\frac{\pi}{2}(i-5)+\frac{\pi}{4}))\frac{\Delta x}{\Delta t}$ for $i = 5,6,7,8$. Notice that in the standard LBGK method, the velocities $\mathbf{e}_i$ are such that after a single time-step the particles travel to the neighboring lattice point along link i. In our current formulation this is not necessarily the case. In section IV we

will discuss this point in some more detail. The convection operation, A_i can be now simply rewritten into the following form,

$$A_i = \mathbf{e}_i \cdot \nabla f_i = e_{ix} \frac{\partial f_i}{\partial x} + e_{iy} \frac{\partial f_i}{\partial y}.$$

By substituting the appropriate finite-difference expressions, we get a fully discrete formulation for A_i.

The time update is performed using a second-order Runge-Kutta scheme. Here we first calculate at each time step, t, the particle densities at time-step $t + \frac{1}{2}$, as follows,

$$f_i(t + \frac{1}{2}) = f_i(t) + \frac{\Delta t}{2}(-A_i(t) + \Omega_i(t)). \tag{A.4}$$

The particle densities at time-step $t+1$ are computed by combining the solutions of time-steps t and $t + \frac{1}{2}$,

$$f_i(t+1) = f_i(t) + \frac{\Delta t}{2}(-A_i(t + \frac{1}{2}) + \Omega_i(t + \frac{1}{2})). \tag{A.5}$$

The collision operator is defined as,

$$\Omega_i(t) = -\frac{1}{\tau}(f_i - f_i^{eq}), \tag{A.6}$$

and in the case of the standard nine-speed LBGK method the equilibrium distribution, f_i^{eq}, is defined as,

$$f_i^{eq} = \rho\, w_i(1 + \frac{3(\mathbf{e}_i \cdot \mathbf{u})}{c^2} + \frac{9(\mathbf{e}_i \cdot \mathbf{u})^2}{2c^4} - \frac{3\mathbf{u}^2}{2c^2}), \tag{A.7}$$

where $c = \frac{\Delta x}{\Delta t}$, w_i is $\frac{4}{9}$ for the rest-particle, $\frac{1}{9}$ for the horizontal and vertical links and $\frac{1}{36}$ for the diagonal links, respectively. The hydrodynamic moments, density ρ, and velocity $\mathbf{u}$ are defined as,

$$\rho = \sum_{i=0}^{N} f_i \qquad \mathbf{u} = \frac{\sum_{i=1}^{N} f_i \mathbf{e}_i}{\rho}.$$

For the nine-speed LBGK method the speed of sound, c_s, and the kinematic viscosity, ν, are given by $c_s = \sqrt{\frac{1}{3}}\frac{\Delta x}{\Delta t}$ and $\nu = \frac{\tau - \frac{1}{2}}{3}\frac{\Delta x^2}{\Delta t}$, respectively [80]. The term $-\frac{\frac{1}{2}}{3}\frac{\Delta x^2}{\Delta t}$ in the expression for the kinematic viscosity of LBGK accounts for numerical viscosity. Due its special form it can be included as a correction factor in the simulated viscosity provided that the molecular velocities are such that particles travel to one of their neighboring points at each time step. Consequently the Lattice-BGK method is second-order accurate in space and time although it is based on first-order discretization schemes. However, if the molecular velocities are decoupled from the lattice one has to use second-order space and time discretization schemes to guarantee second-order accuracy, and the kinematic viscosity is then given by, $\nu = \frac{\tau}{3}\frac{\Delta x^2}{\Delta t}$ [29].

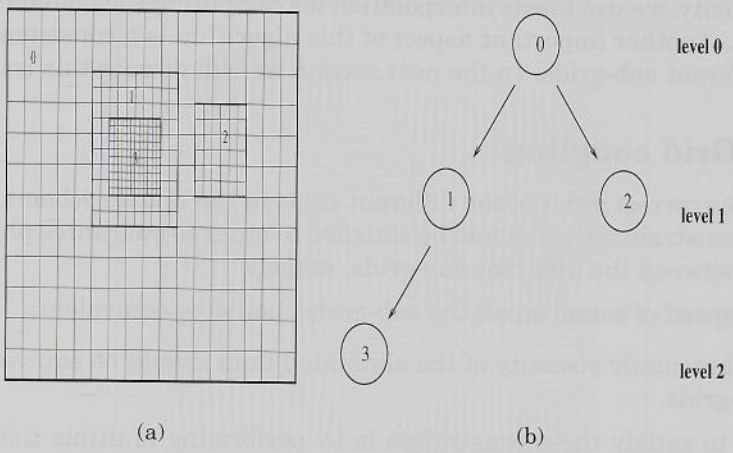

Figure A.1: On the left an example of a nested grid is shown and on the right the corresponding hierarchical structure is depicted

A.4 Nested grids

A.4.1 Algorithm

The nested grid method is organized in a hierarchical way. The parent grid (with the coarsest grid resolution) may contain a number of child nodes with finer resolutions. These child nodes can be parent nodes of sub-grids with a finer grid resolution (see Fig. A.1). In the following we assume that the composite grid is built up of N different levels $(0..N-1)$. The coarsest grid is the parent node and the grids with the finest resolution are the leaves of the tree. In the beginning of the simulations all the sub-grids are initialized to a uniform flow field. The time evolution of the Boltzmann scheme for the composite grid consists of the following phases (top down fashion),

1. The solution on the coarsest grid is first computed (level 0);

2. then the boundary conditions for the level 1 grids are interpolated from their parent sub-grid. We call this step 'the coarse to fine interpolation' and the solution on this level is advanced in time;

3. step 2 is repeated for levels 2 to $N-1$ recursively;

4. subsequently the boundary conditions for the level $N-2$ sub-grids are interpolated from the computed flow field of the $N-1$ grid ('fine to coarse interpolation') and the new values are computed as described in the previous step;

5. finally the same procedure is applied for level $N-2$ to level 0.

For simplicity, we use linear interpolation for computing the boundaries on the sub-grids. Another important aspect of this algorithm is a consistent coupling of the different sub-grids. In the next section we will discuss this issue.

A.4.2 Grid coupling

Besides the correct order of the different steps in the update scheme, there are physical constraints that should be satisfied in order to guarantee physical consistency between the different sub-grids, namely

- the speed of sound on all the sub-grids should be equivalent;
- the kinematic viscosity of the simulated fluid should be equivalent on all sub-grids.

One way to satisfy these constraints is by performing multiple time steps on the fine grids. For example if we consider two levels of refinements, a coarse and a fine one, with $\Delta x^{fine} = \frac{\Delta x^{coarse}}{2}$ (refinement factor is 2), then in order to simulate the same speed of sound on both grids we can take $\Delta t^{fine} = \frac{\Delta t^{coarse}}{2}$. Consequently, the relaxation parameter should also be rescaled such that the viscosity is the same on both grids. Additionally, the distribution functions also need to be rescaled. This approach has been proposed by Fillipova and Hanel [122].
An alternative way to couple the grids consistently is by making the molecular velocities $\mathbf{e}_i$ grid dependent (in lattice units)

$$\mathbf{e}_i = \alpha(cos(\frac{\pi}{2}(i-1)), sin(\frac{\pi}{2}(i-1)))\frac{\Delta x}{\Delta t}$$

for $i = 1,2,3,4$ and

$$\mathbf{e}_i = \alpha\sqrt{2}(cos(\frac{\pi}{2}(i-5)+\frac{\pi}{4}), sin(\frac{\pi}{2}(i-5)+\frac{\pi}{4}))\frac{\Delta x}{\Delta t}$$

for $i = 5,6,7,8$, where the α-parameter allows for an equal scaling of all discrete velocities.
Using mass and momentum conservation, $\rho\mathbf{u} = \sum_{i=0}^{N} f_i^{eq}$ and $\rho\mathbf{u} = \sum_{i=0}^{N} f_i^{eq}\mathbf{e}_i$, one can show that the equilibrium state should now be defined as,

$$f_i^{eq} = \rho\, w_i(1 + \frac{3(\mathbf{e}_i \cdot \mathbf{u})}{c^2\alpha^2} + \frac{9(\mathbf{e}_i \cdot \mathbf{u})^2}{2c^4\alpha^4} - \frac{3\mathbf{u}^2}{2c^2\alpha^2}). \tag{A.8}$$

This idea has similarities to the method first proposed by Koelman [123]. The speed of sound and the kinematic viscosity are given by [123],

$$c_s = \sqrt{\frac{1}{3}}\frac{\alpha\Delta x}{\Delta t} \tag{A.9}$$

$$\nu = \frac{\tau}{3}\frac{\alpha^2\Delta x^2}{\Delta t^2}. \tag{A.10}$$

Keeping the speed of sound and the kinematic viscosity equal on each grid resolution is simply accomplished by taking $\alpha\Delta x$ constant on each grid. Notice that the molecular velocities and the time step are completely determined by stability constraints on the fine grids.

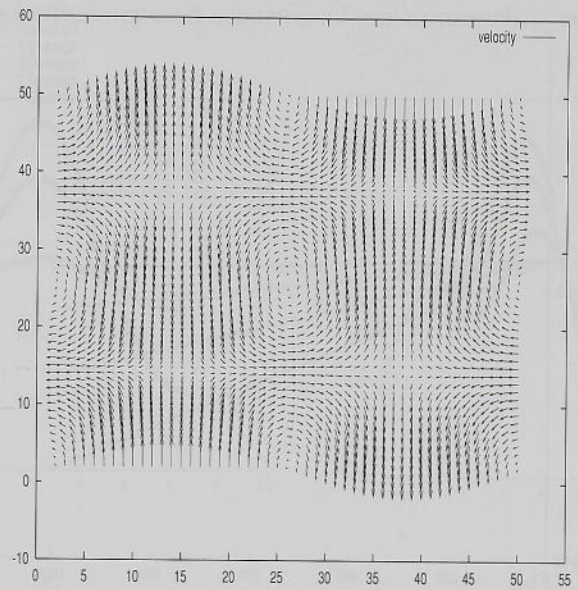

Figure A.2: The initial velocity u_x in the Taylor Vortex benchmark.

A.5 Preliminary results

We study the time dependent two-dimensional Taylor vortex problem (see Fig. A.2). In this benchmark the velocity (u_x, u_y) is initialized as follows,

$$u_x(x,y) = -u_0 cos(k_1 x) sin(k_2 y) \qquad and \qquad u_y(x,y) = u_0(\frac{k_1}{k_2}) sin(k_1 x) cos(k_2 y),$$

where k_1 and k_2 are given by $k_1 = \frac{2\pi m}{L}$ and $k_2 = \frac{2\pi n}{W}$. Here L and W are the dimensions of the systems. In this test case there is no driving force and the flow boundaries are periodic. It can be shown that the velocities will decay as follows

$$u_x(x,y,t) = -u_0 exp^{(-\nu t(k_1^2+k_2^2))} cos(k_1 x) sin(k_2 y), \tag{A.11}$$

$$u_y(x,y,t) = u_0(\frac{k_1}{k_2}) exp^{(-\nu t(k_1^2+k_2^2))} sin(k_1 x) cos(k_2 y). \tag{A.12}$$

We first verify the relation between the viscosity and the scaling factor α (Eq. A.10). These tests are performed on a single grid. The relaxation parameter $\tau = 1$ and $L = W = 50$. In Fig. A.3 we show the velocity at point $(\frac{L}{4}, \frac{W}{2})$ in the grid as a function of time for $\alpha = 0.1, 0.2, 0.3$ and 0.4. We clearly see that there is an exponential decay in time for each α. Moreover, the computed value of the decay exponent is in 1% agreement with the analytical value. In this figure we included the results obtained by the second-order central difference/Runge-Kutta methods. Similar results have been found for the second-order upwind/Runge-Kutta schemes (data not shown).

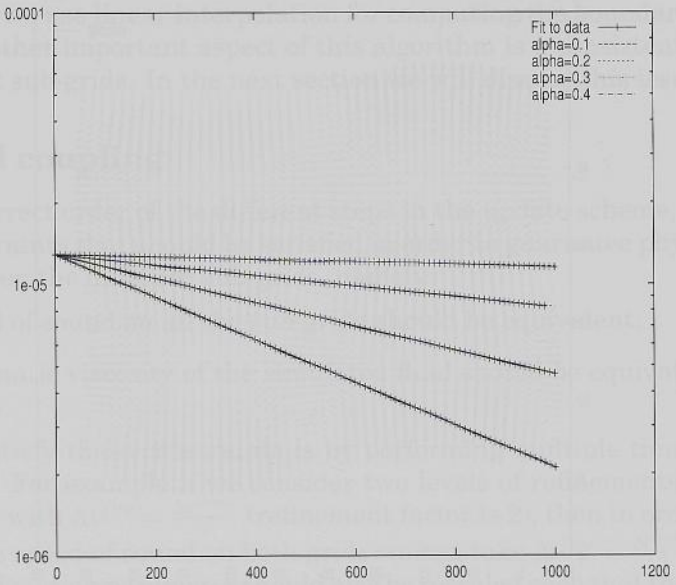

Figure A.3: The decay of the velocity in time at coordinate $(\frac{L}{4}, \frac{W}{2})$ for different values of α.

As a first validation of the method on nested grids, we studied the Taylor vortex evolution on computational lattice built up of a coarse and a fine grid. The fine grid is placed at the center of the domain. This choice is rather arbitrary because in this problem there are no clear regions with large differences in the computational error. However, this benchmark is still useful because it can demonstrate the consistency of the grid coupling and provide some insight in the error due to the first-order interpolation techniques used to compute the boundaries of the sub-grids. In these simulations we only allow coupling between the coarse to fine grid. In Fig. A.4.a we show the velocity profiles after 100 time steps at three lines parallel to the horizontal axes. We clearly see that there is a very good agreement between the solutions obtained on the fine and coarse grids. The error which is defined as the difference between the computed and the analytical value is shown in Fig. A.4.b. In the ideal case it is expected that the error is approximately four times smaller on the fine grid. However, we found that the error obtained on both grid resolutions are very close to each other. This might be due to the first-order interpolation schemes and the fact that in this test-case we do not refine in regions with high errors. These results still show that the physical behavior on the different grids is consistent. Similar results are found for other time steps $t = 1000$ and $t = 2000$ time-steps (see Figs. A.5 and A.6).

As argued above in this test case there are no clear regions with sharp error gradients. Moreover the test-case itself is simple. Thus more simulations including nonlinear flow problems need to be performed in order to demonstrate

the computational efficiency and accuracy of our approach.

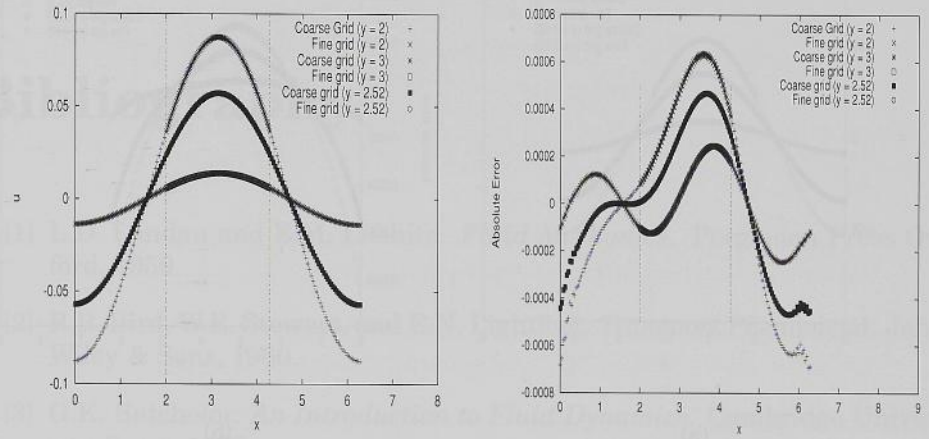

(a) (b)

Figure A.4: The velocity at three lines parallel to the x-axis on both grid resolutions and the corresponding absolute errors at $t = 100$. The region between the dashed lines contains the fine grid.

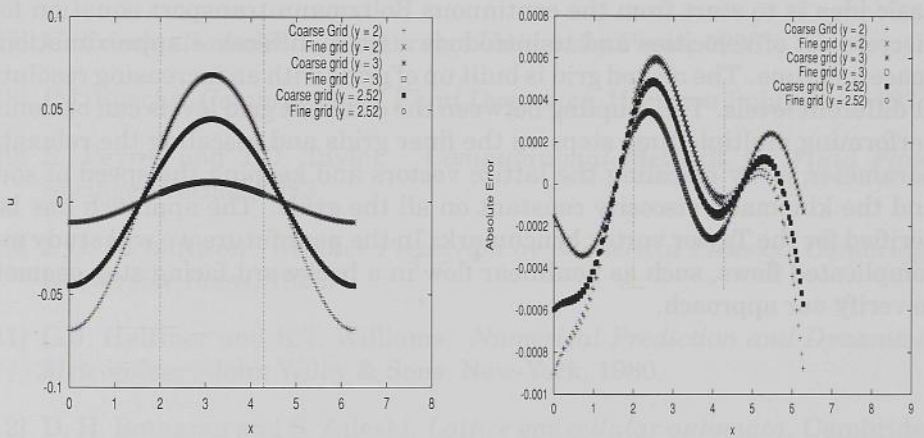

(a) (b)

Figure A.5: The velocity at three lines parallel to the x-axis on both grid resolutions and the corresponding absolute errors at $t = 1000$. The region between the dashed lines contains the fine grid.

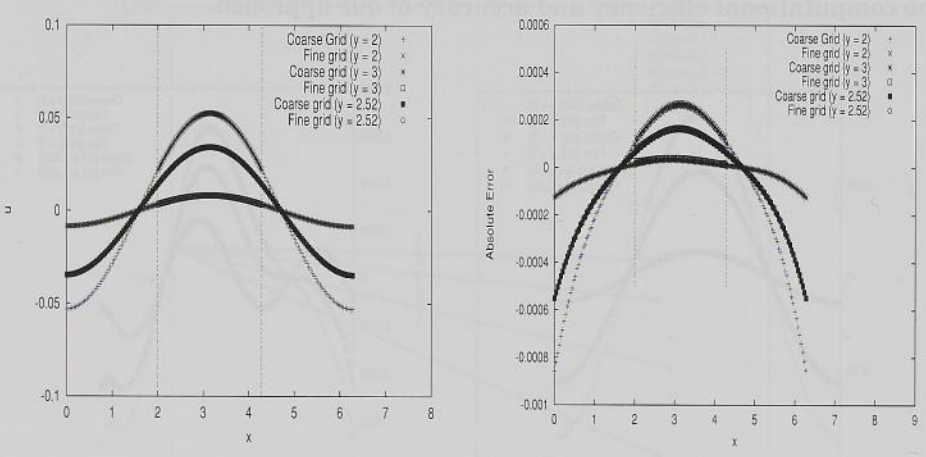

(a) (b)

Figure A.6: The velocity at three lines parallel to the x-axis on both grid resolutions and the corresponding absolute errors at $t = 2000$.The region between the dashed lines contains the fine grid.

A.6 Conclusion and Future Work

In this work we studied Lattice Boltzmann models on nested grids in 2D. The basic idea is to start from the continuous Boltzmann transport equation for a discrete set of velocities and to introduce a finite-difference approximation in space and time. The nested grid is built up of grids with an increasing resolution at different levels. The coupling between the different grid levels can be done by performing multiple time steps on the finer grids and rescaling the relaxation parameter, or by rescaling the lattice vectors and keeping the speed of sound and the kinematic viscosity constant on all the grids. The approach has been verified for the Taylor vortex benchmark. In the near future we will study more complicated flows, such as nonlinear flow in a backward facing step geometry, to verify our approach.